J Therm Anal Calorim (2010) 100:839–845
DOI 10.1007/s10973-010-0711-2

Size and purity of gold nanoparticles changes with different types of thiolate ligands

Weijuan Jia · Jessica McLachlan · Jiayan Xu · S. Holger Eichhorn

CTAS2009 Special Chapter

Abstract Gold nanoparticles (Au-NPs) were prepared by a surfactant-free single-phase reduction of hydrogen tetrachloroaurate(III) hydrate in the presence of different organic thiol ligands. Sizes, size distributions, and crystallinity of the Au-NPs were determined by high-resolution transmission electron microscopy and powder X-ray diffraction, whereas thermogravimetric analysis provided information on the organic ligand-to-gold ratios as well as amounts of contaminants. A systematic decrease in size with increasing conical bulk of the thiolate ligand is observed but large size distributions and contamination of the generated Au-NPs prohibit detailed mechanistic studies. A first-generation Fréchet dendron thiol produced the smallest and cleanest Au-NPs of the narrowest size distribution.

Keywords Chemical · Gold · Nanoparticles · Mass spectrometry · Solution synthesis · Transmission electron microscopy (TEM) · Thermogravimetric analysis (TG) · UV–Vis spectroscopy · X-ray diffraction

Introduction

Monolayer-protected soluble noble metal nanoparticles (NPs) have become ubiquitous building blocks for nano-sized materials and are commercially available as markers in biochemistry and molecular biology [1–6]. Stable NPs of noble metals protected by thiolate ligands have been prepared directly or via replacement of weak sacrificial ligands such as alkyl amines. Direct synthesis may be conducted by two-phase [7] and single-phase methods [8, 9] as well as with and without the aid of surfactants. The average size and size distribution of the obtained NPs crucially depends on the reaction conditions. In particular, the gold-to-thiol, gold-to-reducing agent, and gold-to-phase transfer agent ratios, as well as the addition rate of the reducing agent and the reaction temperature have been shown to affect the size and size distributions of the generated NPs [2, 4, 10–13].

It is generally accepted that the Au^{3+} ions are first reduced to Au^{+} ions by thiols that are oxidized to disulfides [14–16]. The generated Au^{+} ions are assumed to form linear oligomers bridged by thiolate anions and these oligomers are then reduced by the added reducing agent to gold NPs. In fact, recent single-crystal structures of thiol-protected gold NPs show that the crystallized NPs are passivated by networks of Au^{+} thiolate oligomers and not by individual thiolate ligands bond directly to the outer shell atoms of the gold cluster [17, 18]. However, the exact growth mechanism of the gold clusters, the formation of the thiolate anions, and the involvement of other components of the reaction mixture, such as surfactants, remain uncertain despite recent advances in knowledge [4, 19, 20].

Also uncertain is whether different thiolate ligands affect growth of metal NPs differently. It may be expected, for example, that thiolate ligands of large steric bulk are more effective in protecting the curved surfaces of the metal NPs [14]. Linear alkanethiols of different length have produced gold and other metal NPs of similar core sizes and size distributions, under both single- and two-phase conditions, even though the stability of the NPs increases with increasing length of the alkane chain [21]. Ligands containing aromatic units, such as 4-thiocresol,

W. Jia · J. McLachlan · J. Xu · S. H. Eichhorn (✉)
Department of Chemistry and Biochemistry, University of Windsor, Windsor, ON, Canada
e-mail: eichhorn@uwindsor.ca

2-naphthalenethiol, and aliphatic thiols that contain phenyl rings, generated Au-NPs of larger average core sizes (2–3 nm) and wider size distributions than hexanethiolate-passivated Au-NPs (1.7 nm) prepared under identical two-phase conditions [22–25]. Thiophenol, however, generated much larger Au-NPs of 6.5 nm average core diameter.

Inconclusive results have been reported for Au–NPs protected by dendritic thiolates and prepared by two-phase protocols. Phenyl containing Fréchet-type dendron thiols of different generations were investigated by Kim et al. [26] and Gopidas et al. [27]. Both reported average gold core diameters between 2 and 3 nm, independent of the size/generation of the dendron, but contradictory results regarding their particle size distributions. A large dependence of the Au core size on the size/generation of the dendron was observed by Wang et al. [28] who utilized a weakly binding 4-pyridone unit instead of a strongly binding thiol. Surprisingly, the core sizes increased with the sizes/generations of the dendrons and this increase is reasoned with increasing void space in the center of spherically packed dendrons.

NPs prepared under surfactant-free single-phase conditions are not contaminated by the ionic phase transfer agents and surfactants [29, 30] but may contain other ionic side-products and usually have large size distributions [31]. However, the effect of different ligands on the growth of Au-NPs may be best studied under surfactant-free single-phase conditions because the presence of phase transfer agents and other surfactants is likely to diminish the influence of thiolate ligands on the particle growth.

Presented herein is a comparative study of different thiolate ligands (Scheme 1) in the preparation of Au-NPs by a surfactant-free single-phase method. We have previously reported that these ligands have no systematic effect on the size and size distribution of Pd NPs [32] and report here a distinct effect of the different thiols on the sizes, size distributions, and purity of Au-NPs prepared by a similar method. A reduction in size with increasing size/generation of dendron thiols has also recently been reported by Love et al. [33] for Au–NPs prepared by a surfactant-free single-phase method.

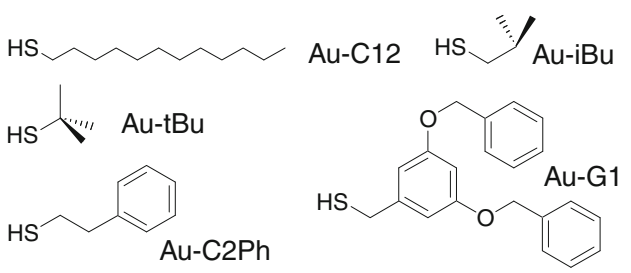

Scheme 1 Structures of investigated thiols and the names of Au-NPs derived from them

Experimental

Materials

All chemicals were used as-received from Sigma Aldrich Canada (Oakville, ON, Canada) and Strem Chemicals, Inc. (Newburyport, MA, USA). THF was purified and dried by a solvent purification system from Innovative Technology Inc. (Newburyport, MA, USA). 1,3-*Bis*-benzyloxy-5-bromomethyl-benzene was prepared in analogy to a procedure described earlier [34] and its reaction with thioacetic acid in the presence of cesium carbonate followed by a treatment with lithium aluminum hydride gave the final product 3,5-*bis*-benzyloxy-phenyl-methanethiol (Au-G1) as a pale yellow solid.

General synthesis and purification of the gold NPs

Hydrogen tetrachloroaurate(III) hydrate (0.306 g, 1 mmol) was dissolved in 15 mL of dry THF and stirred under Ar for 15 min. 2.5 eq. of thiol was added and the mixture was stirred for another 30 min. 15 mL of Superhydride® solution (1 M in THF, 15 mmol of lithium triethylborohydride) was added over 30 min via a syringe pump under Ar. The mixture was stirred for another 2 h, quenched by the addition of dry ethanol (30 mL), and refrigerated for 12 h. The precipitated NPs were filtered off with a 0.2-μm PTFE membrane filter, washed with ethanol (95%), redissolved in THF (5 mL), and again precipitated by the addition of ethanol (30 mL). The final precipitate was collected on a PTFE membrane filter and dried in vacuum (4 mbar) for 24 h. Yields of dried NPs based on gold salt were Au–C12 (72%), Au–C2Ph (68%), Au–iBu (42%), Au–tBu (31%), Au–G1 (89%).

Removal of basic inorganic salts such as Li_2CO_3 was achieved by precipitation from acidic THF solutions [31] but only Au-C12 and Au-C2Ph are stable to these conditions and Au-G1 did not require any removal of salts.

Characterization of NPs

UV–Vis spectroscopy, high-resolution transmission electron microscopy (HR-TEM), powder X-ray diffraction (XRD), and thermogravimetric analysis (TG) were performed as described previously [32].

Results and discussion

Synthesis of gold NPs

Reaction conditions and work-up were similar to the one-phase procedure reported by Yee et al. [9] and were identical for all reactions. Tetrachloroaurate(III) hydrate was reacted

with 2.5 eq. of thiol in THF and then reduced by the addition of lithium triethylborohydride at room temperature under argon. Fractionation of the obtained NPs was kept to a minimum during the work-up. The different thiols were chosen for their differences in steric bulk with regard to the thiolate binding site. The conical bulk of the ligands increases as follows: dodecyl thiol < ethylphenyl thiol < isopropyl thiol < tert-butyl thiol < 3,5-dibenzyloxy-benzyl thiol.

Characterization of Au-NPs by UV–Vis spectroscopy, TEM, and XRD

UV–Vis spectroscopy of the reaction solutions provided the first evidence of differences in particle sizes (Fig. 1).

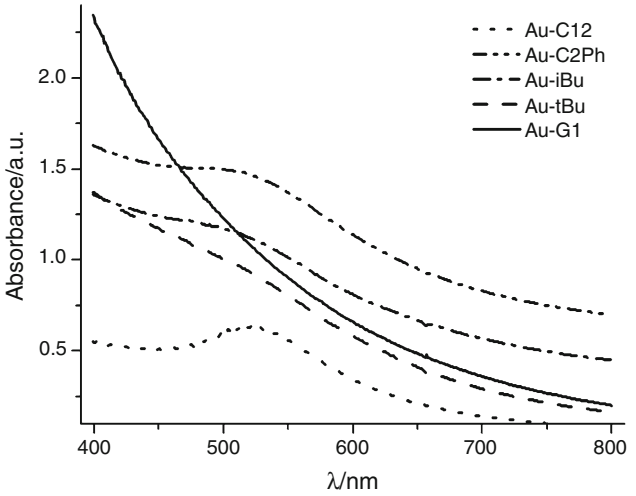

Fig. 1 Absorption spectra of as prepared Au-NPs in THF solution (different concentrations). Surface plasmon absorption maxima (λ_{max} 505–525 nm) were observable for the larger particles Au-C12, Au-C2Ph, Au-iBu (broad), and Au-tBu (very broad) but not for Au-G1

The most intense surface plasmon absorption peaks were obtained for Au-C12 and Au-C2Ph at about $\lambda_{max} = 525$ nm, a typical value for gold NPs in the 2–5 nm size range [10]. Peak shapes broadened and maxima shifted to lower wavelengths for Au-iBu (λ_{max} 508 nm) and Au-tBu (λ_{max} 513 nm), an indication of decreasing size of the gold cores. Au-G1 did not display an observable maximum for the surface plasmon band, which suggests a core diameter below 2 nm. New absorption peaks that have been reported for rather monodisperse Au-NPs of core diameters below 2 nm [35] are not resolved for Au-G1 probably due to its larger polydispersity.

HR-TEM images of the Au NP samples confirmed different average sizes and size distributions (Fig. 2). Particles of the largest average core size were obtained for Au-C12 (average = 3.6 nm; size range 1.9–5.0 nm) followed by Au-C2Ph (2.9 nm; 0.8–5.5 nm), Au-tBu (2.1 nm; 0.8–6.0 nm), Au-iBu (2.1 nm; 0.8–3.5 nm), and Au-G1 (1.1 nm; 0.8–2.5 nm and 4.5–5.5 nm (about 2%)). Single-modal distributions were obtained for NPs Au-C12, whereas multimodal size distributions were obtained for Au-C2Ph, Au-tBu, and Au-G1. Au-C2Ph has a trimodal distribution with maxima at 1.4, 2.4, and 4.5 nm, whereas Au-tBu and Au-G1 have bimodal distributions with maxima at 1.4 and 3.4 nm as well as 1.0 and 5.0 nm, respectively.

Au-tBu and Au-iBu were initially soluble in the reaction mixture but became less soluble with time and as isolated solids. This was no surprise since short chain thiols have previously been reported to provide insufficient long-term protection against coagulation [21]. However, we are confident that the observed size distributions have not been altered by the lower stability because a similar size distribution is obtained for Au-tBu NPs that were stabilized by in situ ligand exchange with octadecanethiol, a method we have applied previously [32].

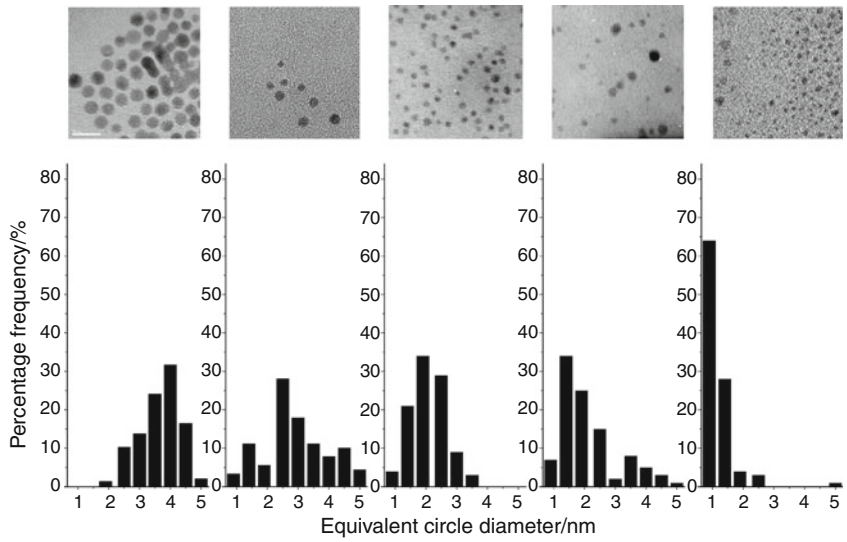

Fig. 2 (*Top*) TEMs of drop-cast films of gold NPs; *from left to right* Au-C12, Au-C2Ph, Au-iBu, Au-tBu, and Au-G1; *scale bar* = 10 nm for all. Their respective size distributions (*bottom*) based on at least 150 clearly separated NPs per sample (about three to eight images)

Powder XRD patterns of the NPs confirmed a crystalline, FCC-like packing of the gold atoms in all NPs but Au-G1 (Fig. 3). The only diffraction peaks observed for Au-G1 were a small-angle peak at $2\theta = 4.1$ and a very broad wide-angle peak at $2\theta = 38.05$ that may be the remnant of the (111) reflection of the gold core. The former peak might be assigned to the periodic packing of NPs with a center-to-center distance of 2.6 nm (110 of bcc or 111 of fcc packing) [13, 36]. An inter-particle distance of 2.6 nm would agree with the determined average core diameter of 1.1 nm and a dendron length of about 1.2 nm if partial interpenetration of the organic layers is assumed [37]. The virtual disappearance of the gold core diffraction peaks is expected for very small NPs and/or NPs with an amorphous core structure.

An increased broadening of the wide-angle diffraction peaks is observed in the order Au-C12 < Au-C2Ph < Au-iBu < Au-tBu, which qualitatively agrees with decreasing core sizes [11]. The large size distributions of the prepared Au-NPs, however, prohibit a detailed analysis because differences in crystal structures are expected for NPs in the 0.8–5 nm range [38].

TG–MS analysis of Au–NPs

TG measurements are employed to study the purity and gold-to-ligand ratio of the Au-NPs. Compounds Au-C12 and Au-C2Ph have been described previously and it was established that additional weight losses may occur at 873 K due to loss of CO_2 of carbonate salt contaminants and above 973 K due to oxidized sulfur species and ionic contaminants [31]. Both NPs could be purified by washing them with dilute acids to verify the presence of contaminants and confirm the thiolate ligand-to-gold ratios. However, only crude NPs are compared here to avoid any changes to the initial sizes of NPs and because NPs Au-iBu and Au-tBu are not stable to the purification steps.

Compound Au-G1 does not show weight loss steps above 773 K, whereas Au-tBu loses 3% of its weight in a step between 833 and 873 K but no further loss occurred above 873 K (Fig. 4). Significant weight loss steps above 973 K are observed for Au-C12, Au-C2Ph, and Au-iBu (8, 41, and 7% of their total weight, respectively) and are due to contaminants. It is uncertain why Au-C2Ph contains such a large amount of contaminants but it is unlikely caused by a more disordered packing of the ligands or the presence of a phenyl group because Au-iBu and Au-tBu and/or Au-G1 should be similarly affected.

Significant differences are also observed in the temperature range of the loss of organic components below 773 K. Compounds Au-C12 and Au-G1 display two distinct steps, a first small loss between 373–443 (0.5%) and 323–423 K (1.5%), respectively, and the main loss of the ligands at on-set temperatures of 463 and 453 K, respectively. Compounds Au-C2Ph and Au-iBu lose their organic content over a wide temperature range starting at about 323 K. Both lose about 2% of their weight up to 453 K, which is the on-set temperature for a steep loss of all the remaining organic content in one step. Only one distinct organic weight loss event is observed for Au-tBu but at a low on-set temperature of 363 K.

Occurrence of a weight loss step requires not only desorption of the ligands, but also their evaporation. Thermal desorption of the thiolate ligands under He will

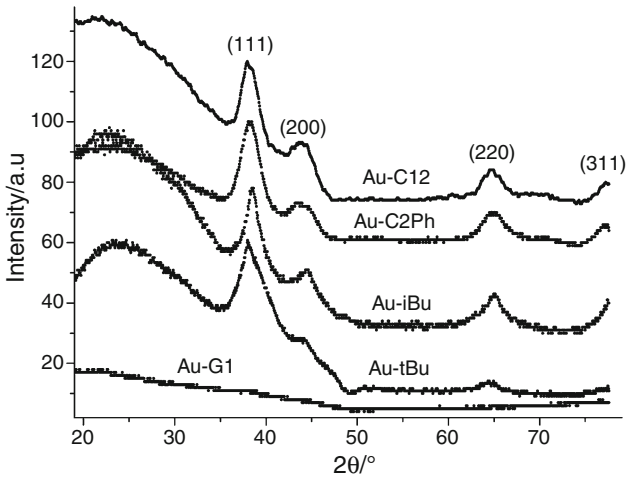

Fig. 3 Wide-angle diffraction data (transmission mode) of Au NP powders in Lindemann capillaries. Presented here are the uncorrected data but the diffraction patterns are vertically offset for clarity. Peak assignment is based on an FCC structure

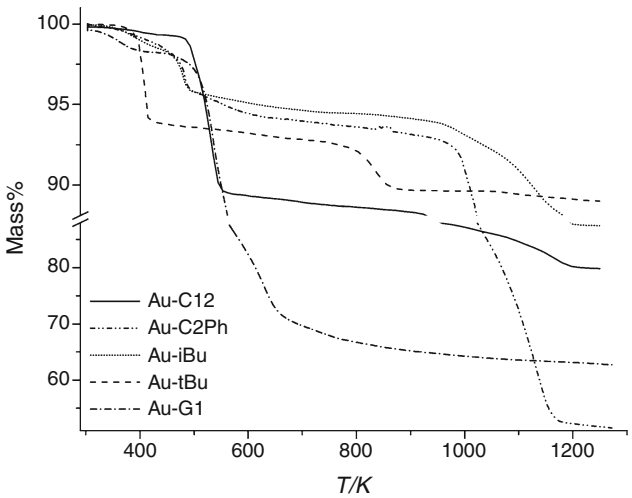

Fig. 4 TG curves of crude Au-NPs at a heating rate of 5 K/min to 773 K and 10 K/min from 773 to 1273 K. Mass losses below 773 K are attributed to the loss of the thiolate ligands and organic contaminants, losses above 773 K to the decomposition of inorganic contaminants such as Li_2CO_3

produce disulfides and may occur below 373 K but only the ligands of Au-iBu and Au-tBu form disulfides that are sufficiently volatile to cause a significant weight loss below 373 K. Weight losses below 373 K in compounds Au-C12, Au-C2Ph, and Au-G1 are likely caused by the evaporation of small amounts of solvent that remained in the vacuum-dried samples because their disulfides formed by desorption neither evaporate at sufficient rates nor decompose at these temperatures.

The average total number of Au atoms and the percentages of Au atoms at the surfaces of the NPs are estimated following a method proposed by Heath and Gelbart [11]. Radii of the gold cores are derived from the average diameters determined by TEM. The number of thiolate molecules per average NP is calculated based on the average total number of Au atoms per NP, the molecular weights of Au and the thiolates, as well as the percentage weight content of thiolates corrected for content of inorganic contaminants as determined by TG (Table 1). Surface gold-to-thiolate ratios of Au-C12 and Au-C2Ph calculate to 2.5 and 2.4, respectively, and are consistent with values that have been reported for alkanethiolate-protected Au-NPs of similar size [10]. Larger ratios are obtained for Au-G1 (2.8), Au-tBu (2.9), and Au-iBu (3.8).

Most of the reported ratios for Au-NPs protected with linear alkanethiolates are between 1.5 and 2.6 and a surface gold-to-thiolate ratio of 3 is found in self-assembled monolayers on two-dimensional gold (111) surfaces [10]. This difference between 2D and 3D monolayers of thiolates has been reasoned with thiolates that might bond to only 2 or 1 Au atoms at edges and corners of the polyhedra, respectively [21]. Thus, decreasing ratios are expected for decreasing particle sizes as their ratio of edge/corner-to-facet gold atoms increases [10] but the opposite change is observed here for the smaller NPs Au-G1, Au-tBu, and Au-iBu.

The observed increase in the surface gold-to-thiolate ratio may be explained with an increase in steric bulk for a change from *n*-alkanethiolate to branched alkanethiolate or dendron thiolate ligands that prevent the thiolate groups from packing closely at the Au surface [14, 27]. The calculated surface gold-to-thiolate ratios for Au-G1 and Au-tBu compare reasonably well with reported structures such as $Au_{55}(PPh_3)_{12}Cl_6$ [39]. However, the unusually large ratio obtained for Au-iBu is likely an artifact caused by insufficient stability of Au-iBu. TG measurements are performed on dried powders that may contain fused NPs, whereas size distributions only include soluble as-prepared NPs transferred onto TEM grids.

Despite these experimental imperfections, a clear decrease in size of the NPs with increasing bulk of the ligand is observed and the question arises what causes the differences in particle sizes. A reduction in size is expected due to differences in thermodynamic stability because smaller NPs have a higher curvature and should preferentially accommodate thiolates of more conical bulk. However, differences in thermodynamic stability are unlikely the reason for the observed size effect because a thermodynamically controlled growth should produce narrower size distributions and Pd NPs prepared with the same ligands using a similar procedure did not show a correlation between conical bulk and particle size but much narrower size distributions [32]. The absence of an effect on Pd NPs also disfavors differences in growth kinetics of the NPs as a plausible reason. A growing metal nucleus containing bulkier ligands may be expected to be more effectively shielded from approaching metal atoms and clusters.

An important difference between the formation processes of Au-NPs and Pd NPs in the presence of organic thiols is the intermediate formation of Au(I) thiolate oligo/polymers [15, 16]. Recent studies on single crystals even

Table 1 Calculated values of surface gold-to-thiolate ratios derived from the average core size and organic ligand content determined by TEM and TG, respectively

Au NP	Average diameter/nm	Content of SR[a]/wt%	$Au^{b}_{(total)}$	$\%Au^{b}_{(surf.)}$	SR/NP[c]	$Au_{(surf.)}/SR^{d}$
Au-C12	3.6	12.4[e]	1437	34.6	199	2.5
Au-C2Ph	2.9	10.9	751	41.6	132	2.4
Au-iBu	2.1	5.9	285	53.8	40	3.8
Au-tBu	2.1	7.8	285	53.8	53	2.9
Au-G1	1.1	32.9[e]	41	81.7	12	2.8

[a] Content of thiolate groups based on TG in wt% regarding the total weight minus the content of inorganic contaminants

[b] Average total number of gold atoms per NP and % of gold atoms at surface sites calculated by Heath's and Gelbart's method based on average core diameters derived from TEM

[c] Average number of thiolate molecules per NP calculated from the weight loss in TG and $Au_{(total)}$

[d] Ratio between calculated average number of gold atoms at the surface and thiolate molecules per NP

[e] This value was also corrected for the small content of solvent that evaporated below 373 K

suggest that these polymers can actually form the protective layer around clusters of reduced Au atoms [17, 18]. Our hypothesis is that the structure of the formed Au(I) thiolate oligo/polymers is affected by the differences in conical bulk of the thiolate ligands and that these structural changes influence the growth of the Au-NPs. It is worthwhile mentioning here that we did not observe a systematic size effect for higher initial contents of thiol ligands (3.5 and 4.5 eq.), although NPs Au-G1 were consistently the smallest.

Conclusions

Thiols of increasing conical bulk generate smaller Au-NPs if prepared by the given surfactant-free single-phase method. A size control due to differences in the thermodynamic stabilities or growth kinetics of the NPs is unlikely because no such effect was observed for Pd NPs prepared under similar conditions. Similarly unlikely is that the observed contaminants influence the size of the NPs since no systematic dependence of the sizes on the content of contaminants was found. We propose that the intermediate formation of Au(I) thiolate oligo/polymers is affected by the bulk of the ligands and causes differences in cluster growth. However, more detailed experimental studies are required for elucidating the growth mechanism and the underlying reasons for the observed size effect.

Acknowledgements The authors thank the National Science and Engineering Research Council (NSERC) of Canada, the Canadian Foundation for Innovation (CFI), the Ontario Innovation Trust (OIT), the Ontario Centres of Excellence (OCE), and Barrick Gold for funding. McLachlan thanks NSERC for undergraduate summer research awards (USRA). We are also grateful to Fred Pearson at McMaster University for TEM measurements.

References

1. Brust M, Kiely CJ. Some recent advances in nanostructure preparation from gold and silver particles: a short topical review. Colloids Surf A. 2002;202:175–86.
2. Daniel MC, Astruc D. Gold nanoparticles: assembly, supramolecular chemistry, quantum-size-related properties, and applications toward biology, catalysis, and nanotechnology. Chem Rev. 2004;104:293–346.
3. Schmid G, Corain B. Nanoparticulated gold: syntheses, structures, electronics, and reactivities. Eur J Inorg Chem. 2003;2003:3081–98.
4. Burda C, Chen X, Narayanan R, El-Sayed MA. Chemistry and properties of nanocrystals of different shapes. Chem Rev. 2005;105:1025–102.
5. Rao CNR, Kulkarni GU, Thomas PJ, Edwards PP. Metal nanoparticles and their assemblies. Chem Soc Rev. 2000;29:27–35.
6. Schmid G, editor. Nanoparticles. Weinheim: Wiley-VCH; 2004.
7. Brust M, Walker M, Bethell D, Schiffrin DJ, Whyman R. Synthesis of thiol-derivatized gold nanoparticles in a 2-phase liquid–liquid system. Chem Commun. 1994;801–2.
8. Yee C, Scotti M, Ulman A, White H, Rafailovich M, Sokolov J. One-phase synthesis of thiol-functionalized platinum nanoparticles. Langmuir. 1999;15:4314–6.
9. Yee CK, Jordan R, Ulman A, White H, King A, Rafailovich M, et al. Novel one-phase synthesis of thiol-functionalized gold, palladium, and iridium nanoparticles using superhydride. Langmuir. 1999;15:3486–91.
10. Hostetler MJ, Wingate JE, Zhong CJ, Harris JE, Vachet RW, Clark MR, et al. Alkanethiolate gold cluster molecules with core diameters from 1.5 to 5.2 nm: core and monolayer properties as a function of core size. Langmuir. 1998;14:17–30.
11. Leff DV, Ohara PC, Heath JR, Gelbart WM. Thermodynamic control of gold nanocrystal size: experiment and theory. J Phys Chem. 1995;99:7036–41.
12. Quiros I, Yamada M, Kubo K, Mizutani J, Kurihara M, Nishihara H. Preparation of alkanethiolate-protected palladium nanoparticles and their size dependence on synthetic conditions. Langmuir. 2002;18:1413–8.
13. Whetten RL, Shafigullin MN, Khoury JT, Schaaf TG, Vezmar I, Alvarez MM, et al. Crystal structures of molecular gold nanocrystal arrays. Acc Chem Res. 1999;32:397–406.
14. Love JC, Estroff LA, Kriebel JK, Nuzzo RG, Whitesides GM. Self-assembled monolayers of thiolates on metals as a form of nanotechnology. Chem Rev. 2005;105:1103–70.
15. Groenbeck H, Walter M, Haekkinen H. Theoretical characterization of cyclic thiolated gold clusters. J Am Chem Soc. 2006;128:10268–75.
16. Howell JAS. Structure and bonding in cyclic thiolate complexes of copper, silver and gold. Polyhedron. 2006;25:2993–3005.
17. Akola J, Walter M, Whetten RL, Hakkinen H, Gronbeck H. On the structure of thiolate-protected Au-25. J Am Chem Soc. 2008;130:3756–7.
18. Walter M, Akola J, Lopez-Acevedo O, Jadzinsky PD, Calero G, Ackerson CJ, et al. A unified view of ligand-protected gold clusters as superatom complexes. Proc Natl Acad Sci USA. 2008;105:9157–62.
19. Chen SW, Templeton AC, Murray RW. Monolayer-protected cluster growth dynamics. Langmuir. 2000;16:3543–8.
20. Biswas K, Varghese N, Rao CNR. Growth kinetics of gold nanocrystals: a combined small-angle X-ray scattering and calorimetric study. Small. 2008;4:649–55.
21. Hostetler MJ, Stokes JJ, Murray RW. Infrared spectroscopy of three-dimensional self-assembled monolayers: N-alkanethiolate monolayers on gold cluster compounds. Langmuir. 1996;12:3604–12.
22. Brust M, Fink J, Bethell D, Schiffrin DJ, Kiely C. Synthesis and reactions of functionalized gold nanoparticles. Chem Commun 1995;1655–6.
23. Chen SW, Murray RW. Arenethiolate monolayer-protected gold clusters. Langmuir. 1999;15:682–9.
24. Johnson SR, Evans SD, Mahon SW, Ulman A. Alkanethiol molecules containing an aromatic moiety self-assembled onto gold clusters. Langmuir. 1997;13:51–7.
25. Venkataramanan M, Ma SG, Pradeep T. 3D monolayers of 1, 4-benzenedimethanethiol on Au and Ag clusters: distinct difference in adsorption geometry with the corresponding 2D monolayers. J Colloid Interface Sci. 1999;216:134–42.
26. Kim M-K, Jeon Y-M, Jeon WS, Kim H-J, Hong SG, Park CG, Kim K. Novel dendron-stabilized gold nanoparticles with high stability and narrow size distribution. Chem Commun 2001;667–8.
27. Gopidas KR, Whitesell JK, Fox MA. Nanoparticle-cored dendrimers: synthesis and characterization. J Am Chem Soc. 2003;125:6491–502.
28. Wang R, Yang J, Zheng Z, Carducci MD, Jiao J, Seraphin S. Dendron-controlled nucleation and growth of gold nanoparticles. Angew Chem Int Ed. 2001;40:549–52.

29. Waters CA, Mills AJ, Johnson KA, Schiffrin DJ. Purification of dodecanethiol derivatised gold nanoparticles. Chem Commun. 2003;540–1.
30. Rowe MP, Plass KE, Kim K, Kurdak C, Zellers ET, Matzger AJ. Single-phase synthesis of functionalized gold nanoparticles. Chem Mater. 2004;16:3513–7.
31. Jia W, McLachlan J, Xu J, Tadayyon SM, Norton PR, Eichhorn SH. Characterization of Au and Pd nanoparticles by high-temperature TGA-MS. Can J Chem. 2006;84:998–1005.
32. Iqbal M, McLachlan J, Jia W, Braidy N, Botton G, Eichhorn SH. Ligand effects on the size and purity of Pd nanoparticles. J Therm Anal Calorim. 2009;96:15–20.
33. Love CS, Ashworth I, Brennan C, Chechik V, Smith DK. Dendritic nanoparticles: the impact of ligand cross-linking on nanocore stability. Langmuir. 2007;23:5787–94.
34. Hawker CJ, Frechet JMJ. Preparation of polymers with controlled molecular architecture—a new convergent approach to dendritic macromolecules. J Am Chem Soc. 1990;112:7638–47.
35. Alvarez MM, Khoury JT, Schaaff TG, Shafigullin MN, Vezmar I, Whetten RL. Optical absorption spectra of nanocrystal gold molecules. J Phys Chem B. 1997;101:3706–12.
36. Sarathy KV, Raina G, Yadav RT, Kulkarni GU, Rao CNR. Thiol-derivatized nanocrystalline arrays of gold, silver and platinum. J Phys Chem B. 1997;101:9876–80.
37. Wang ZL, Harfenist SA, Whetten RL, Bentley J, Evans ND. Bundling and interdigitation of adsorbed thiolate groups in self-assembled nanocrystal superlattices. J Phys Chem B. 1998;102:3068–72.
38. Zanchet D, Hall BD, Ugarte D. Structure population in thiol-passivated gold nanoparticles. J Phys Chem B. 2000;104:11013–8.
39. Schmid G. Large clusters and colloids—metals in the embryonic state. Chem Rev. 1992;92:1709–27.